Competing factors in grain boundary loop shrinkage: two-dimensional hard sphere colloidal crystals

Ziwei Guo (郭子威) and James T. Kindt (jkindt@emory.edu)
Department of Chemistry, Emory University
Atlanta, GA 30322
July 22, 2019, submission to *The Journal of Chemical Physics*

Abstract:

A grain boundary (GB) loop in a two-dimensional solid is the boundary of a domain or grain whose lattice orientation is mismatched with its uniform surroundings. Understanding the factors that influence the rate at which the interior of a GB loop relaxes to the orientation of its surroundings is an important step towards control and predictability of grain coarsening in general. Recent computational and experimental studies looking at the rate of GB loop shrinkage in two-dimensional colloidal hard sphere solids have uncovered contradictory trends: in experiments, GB loops with low misorientation angles shrank the fastest, while in simulations they persisted the longest. In this study, the computational system's behavior is brought into qualitative agreement with the experimental results through increasing the lateral packing pressure, decreasing the domain size, and mimicking the experimental protocol used to form the GB loop. Small GB loops with same misorientation, but displaying either a hexagonal or star-like grain shape depending on the orientation of their six dislocations, are shown to differ in their rates of shrinkage by two orders of magnitude. The evidence suggests that both the barrier to generating new dislocations as well as the pattern of dislocations formed by different GB loop preparation methods will determine which trend is observed.

I. Introduction:

Systems with translational order are often subdivided into grains, domains with different local lattice orientations. In general, as elimination of the interfaces between grains (grain boundaries, or GB) reduces a system's free energy, these systems undergo a process of grain coarsening through which smaller grains (with higher surface/volume ratio) are eliminated.[1] Coarsening often slows down or stops, leaving a polycrystalline material.[2] Understanding the dynamics of grain coarsening and its dependence on the specific properties of the GB involved is important for control and predictability of material microstructure, which in turn influences the bulk behavior of materials.[3] The dynamics of grain coarsening can be affected by many factors, like system pressure, misorientation between GBs, and the presence of impurities.[4] The technical challenges and complexity of interpretation involved with direct experimental probes of the mechanisms of GB dynamics at the atomistic scale are such that modeling has been an essential and ongoing part of understanding these processes.[5] Modeling efforts include both theory and computation[6-14] and experiments on colloidal crystalline systems[15-21] (which, as well as useful model systems, are materials with practical applications of their own[22]) to study these phenomena at more accessible length- and time-scales.

The dynamics of one special type of boundary, the GB loop, has been studied in several works.[8, 11, 12, 14, 18] Trautt *et al.* simulated the isolated cylindrical grain in copper, where they found the dynamics of GB motion and grain rotation is affected by initial misorientation angle θ_0 and temperature.[12] They also employed the dislocation mechanisms to explain the motion of curved GBs.[12] Another MD study by Upmanyu *et al.* shows GB migration and grain rotation occuring

simultaneously, where they observed the grain rotating as a rigid body rather than through dislocation passage through the grain interior.[11]

In a recent simulation study,[23] we have calculated GB stiffness associated with GB at several grain misorientation angles in hard sphere (HS) 2-d solids. The stiffness, a measure of the resistance of the GB to fluctuation, increased with greater misorientation between neighboring grains up to about θ=20° and then appeared to plateau. Because the stiffness did not depend to a discernible degree on GB inclination angle, it can be treated as equal to the line tension or free energy penalty per unit length of the GB. Furthermore, we found that the rate of GB shrinkage - assessed using apparent rates during a Monte Carlo (MC) trajectory - was correlated with the line tension for both single grains embedded in a uniformly oriented background and for a simple four-grain periodic lattice pattern. Whereas the latter result was in good qualitative agreement with experimental results on GB coarsening in a polycrystalline 2-d colloidal system,[17] an experimental report of GB loops in 2-d colloidal solid arrays of silica microspheres showed the opposite trend in the rate of shrinkage versus misorientation angle.[18] In that study, Lavergne *et al.* also demonstrated the dependence of deformation mode (either elastic or plastic) on θ_0 and loop size and related this dependence to topological constraints in the dislocation structure.

Differences in grain size, in packing density or pressure, and in the method of preparation or history of the GB loop are three factors, readily controllable within simulations, that could account for the discrepancy. Other possibilities include deviations of colloidal particle interactions from the idealized hard-sphere model and deviations of Monte Carlo-based effective dynamics from the true experimental behavior. Although Monte Carlo simulation does not produce a trajectory that is directly related to a dynamic algorithm, the evolution of a Monte

Carlo trajectory that uses local displacement moves can give qualitative insight into dynamics. This is particularly true when Brownian dynamics is a good approximation,[24] as expected for colloidal motion.

From the current simulations, including attempts to mimic the laser-tweezer protocol applied experimentally to create GB loops, we have evidence that variations in grain size, system pressure, or method of preparation can all affect the trend in the rate of GB loop shrinkage with varying θ_0. The most unexpected result is that our original protocol for GB loop preparation can produce a structure that resembles the simple hexagonal arrangement of dislocations reported by Lavergne *et al.*,[18] but with a literal twist to the dislocation orientations that makes it much more kinetically stable. The results overall help place the experimental observations in the context of a wider range of possible regimes and conditions.

II. Methods

A. Monte Carlo algorithm

Hard spheres of diameter σ are simulated in a 2-dimensional square box with periodic boundaries. A domain-decomposition scheme is used to parallelize the simulations. The simulation box was divided into either a 2×2 or 12×12 grid with a randomly selected origin, for system size 50 σ×50 σ and 100 σ ×100 σ respectively. MC cycles were performed within each grid square on separate processors, with particles frozen within a zone of distance of 0.5 σ from domain borders. Each MC cycle consists of 20000 regular translation move attempts per grid square, or about 30 move attempts per particle. Each move attempt consists of a displacement chosen from a uniform distribution in the range (-0.05 σ , +0.05 σ)in both x and y. After every

MC cycle, a new origin for the grid is chosen and particles are redistributed among processors so that the border regions are constantly changing. We confirmed that the parallelization scheme did not significantly affect the overall dynamics of grain shrinkage when normalized for number of move attempts per particle.

B. Construction of GB loops by cut-and-paste method

Following our previous simulation of GB loops,[23] the circular domain (with radius R_0 and certain orientation angle respected to the x axis) is inserted into the center of the square domain with a box length L (50σ) and a fixed orientation (aligned to the x axis). Any overlapped particle in the border between the two domains is removed.

C. Construction of GB loops by tweezer-mimic method

A hexagonal array of particles in a square simulation box (with box length 50σ and average 0 orientation respect to the x axis) is used as the initial configuration in the tweezer construction method. Similar to the experiment[18], we aim to induce a torque on a localized region of the 2-d solid. In Monte Carlo simulation, however, we cannot directly apply a force on the particle. Instead, we introduce bias when selecting the directions of random walk. Given a randomly selected particle in system, we perform a rotationally biased move with probability P_{bias}, or a regular translational move with equal probability in any direction. The P_{bias} is set to 0.2 in this work, which is tuned to allow relaxation of local particle arrangements during domain rotation. If the particle is considered for bias move, then the probability of actually making a bias move is P_{mix}, which is a mixed probability of two probability density function P_{LG} and P_G (Fig. 1) depending on the distance from the selected particle to the box center r:

$$P_{LG} = \frac{1}{\sqrt{2\pi\sigma_{LG}^2}} \exp\left[-\frac{(|r|-R_0)^2}{2\sigma_{LG}^2}\right] \quad (1a)$$

$$P_G = \frac{1}{\sqrt{2\pi\sigma_G^2}} \exp\left(-\frac{r^2}{2\sigma_G^2}\right) \quad (1b)$$

The bias probabilities P_{LG} and P_G resemble the Laguerre-Gaussian (LG) beam and Gaussian beam in experiment, respectively,[18] where the LG beam is the main motivation to drive the particle while the Gaussian beam maintains the domain intact during rotation. In contrast to the experiment, we found the domain stays intact under various combinations of standard deviation terms σ_{LG} and σ_G (which tune the strength and width of the probability distribution), even when there is no Gaussian beam at the center. For the best general performance we set σ_{LG}=1.0 and σ_G=3.0 in all our simulations. The overall probability of making a bias move is $P_{bias}P_{mix}$. If selected, the biased move will be an attempt to translate the selected particle to a position along a circular path at fixed *r*. The random move (bias or regular translational) is rejected if it produces an overlap with another particle.

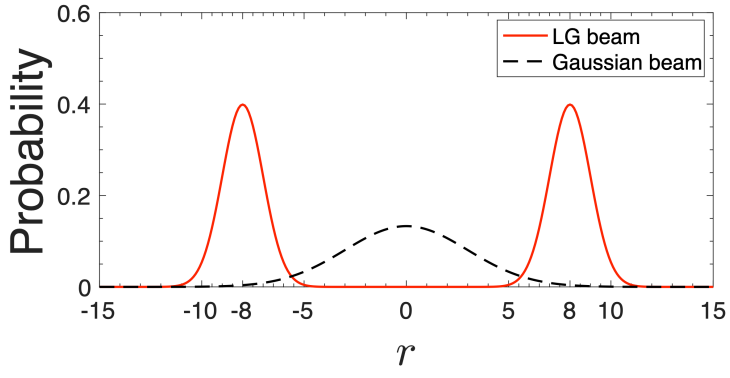

FIG. 1. Probability distribution of bias moves mimicking LG beam and Gaussian beam in simulations with $R_0 = 8\sigma$.

D. Starting structure from experimental report

The Voronoi diagram shown in Figure 3B of Ref. [18] was converted into a set of coordinates for simulation by first manually marking the center of each cell, then scanning in the image. Slight rotation of the coordinates and a scaling (independently in y and z) were performed to maximize alignment of the edges of the coordinate set with a regular 2-d hexagonal lattice (box length 98.1 σ and area fraction 0.82). The 460 positions from the scanned image replaced 460 particles within the lattice as expected for the product of a continuous deformation. Before the dynamical simulation was started, the experimental particle positions were frozen while the surrounding lattice was allowed to equilibrate to remove gaps at the boundary.

E. Mobility measurement from Monte Carlo simulation

The number of particles that remain in the GB loop was tracked over time to assess the shrinking rate, which varies significantly from trajectory to trajectory. For all mobility measurements, 16 shrinking curves starting from different initial structures constructed using different random number seeds were averaged to represent the mean shrinking rate. The bond-orientational order parameter[25] Ψ_6 is used to characterize the local crystalline order of particle j:

$$\Psi_6(\vec{r}_j) = \frac{1}{N_j}\sum_{k=1}^{N_j} e^{i6\Delta\theta_{jk}} \quad (2)$$

where $\Delta\theta_{jk}$ is the angle between the x direction with the vector connecting the central particle j and one of its N_j nearest neighbors, k, within a cutoff 1.5σ. The orientation of the hexagon formed by six neighbors of particle j is $\theta_6 = \arg(\Psi_6)/6$. A particle is classified as belonging to the GB loop if its θ_6 is within 5° of θ_0, or within 2.5° of θ_0 for $\theta_0 = 5°$.

The size of the domain was assessed by the number *N* of particles satisfying this condition and was calculated as a function of the number of MC cycles following the initial preparation. Samples of individual trajectories are shown in Fig. 2 and of averages taken over the 16 trajectories are shown in Fig. 3. Similar plots corresponding to the remaining size and area fraction conditions are given in Supplemental Information, Figs. S1 and S2. Loops of nominal radius 8 σ would be expected to contain 202-210 particles (depending on density) and those of radius 10 σ would contain 316-328 particles. As apparent in Fig. 3, the actual initial domain size (after a single cycle of equilibration) is within 10 particles of the targeted value of 202 for the cut-and-pasted system, but ranged from 175 to 240 particles at different θ_0 in the tweezer-mimic structure, corresponding to deviation of up to 9% in effective radius away from the nominal GB loop radius of 8 σ. Tweezer-rotated grains at the lower pressure in particular show large variability because the rotation process disrupts packing at the boundary, producing an interface with the bulk whose width and degree of disorder grew with increasing misorientation; disrupted boundary particles that are not aligned with the grain interior are not included in the count. To attempt to account for this uncounted area, the rate of shrinkage dN/dt (where t is represented in MC cycles) was obtained by a linear fit over the initial period of the curve (until N reached 50% of its initial value N_0), and then normalized to the initial nominal area of the circle of radius R_0: $M^* = \left(\frac{dN}{dt}\right)({R_0}^2/2N_0)$. It should be noted that the mobility measured from our simulation (in units of σ^2, area loss per MC cycle) cannot directly compared with the number in experiment (in unit of σ^2/s), but we can still compare the relative mobility under different construction methods and conditions.

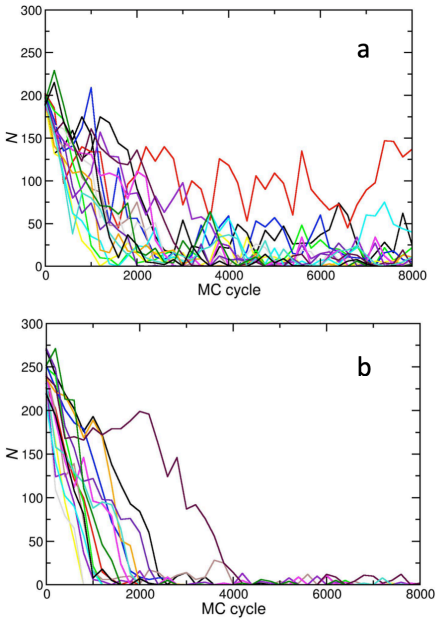

FIG 2. Shrinking curves showing number N of particles inside GB loop created by cut-and-paste method (a) or tweezer-mimic method (b) for initial misorientation 10°, R_0 = 8 σ, at lowest area fraction (0.7825). Different colors represent 16 trajectories initiated with different random number seeds.

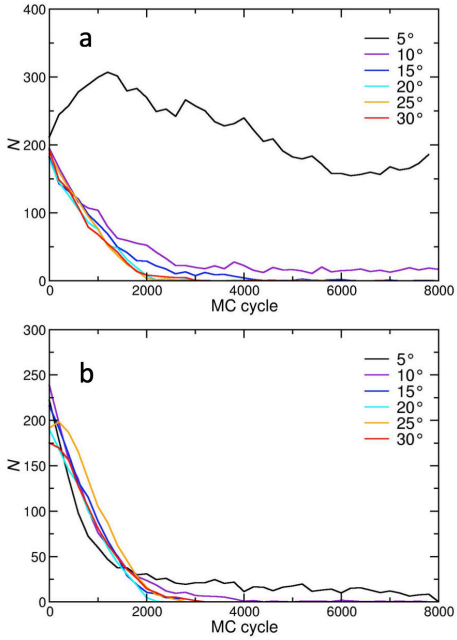

FIG 3. Shrinking curves showing number N of particles inside GB loop, averaged over 16 trajectories, created by cut-and-paste method (a) or tweezer-mimic method (b) at R_0 = 8 σ and lowest area fraction (0.7825). Initial misorientation angles are indicated by colors given in the legend.

Preliminary comparison of M^* determined at different simulation box sizes for R_0=10σ loops (shown in Supplementary Material, Figure S3) showed that the differences between mobilities obtained in 50σ×50σ and 100σ×100σ periodically repeating boxes were small relative to the variations observed upon changing misorientation and loop construction method. Therefore, for computational efficiency, a box size of 50σ×50σ was used for all further rate determinations.

III. Results and discussion:

Wu and Voorhees[14] have described three regimes for the shrinking of a grain boundary loop in phase crystal field simulations. At high misorientation θ, linear decrease in GB loop area with time is controlled by the classical curvature-driven process of transfer of particles between between grains;[1] at low θ, decrease in GB loop area is similarly linear but is accompanied by grain rotation to higher misorientation;[7] and at intermediate θ the process is marked by alternating periods of migration and reaction of dislocations. Unlike in the phase crystal field simulations, the dynamics in the current study are non-deterministic and subject to fluctuations both within a single trajectory and across trajectories. An example is shown in Figure 2; results from the remaining conditions at the same initial misorientation $\theta_0 = 10°$, are shown in Supplementary Material Figure S1. The behaviors of individual trajectories under some conditions show a roughly linear decrease in the area contained by the GB loop with time. In other conditions trajectories are characterized by plateaus of variable duration followed by rapid shrinking. In spite of the wide range of behaviors, for the sake of concision the rate of GB loop shrinkage for all cases is characterized by averaging over the 12 trajectories to yield mean shrinking curves (as

shown in Figure 3 and Supplementary Material Figure S2) and performing a linear fit to the initial period of decrease in number of particles in the grain to obtain a single mobility *M**.

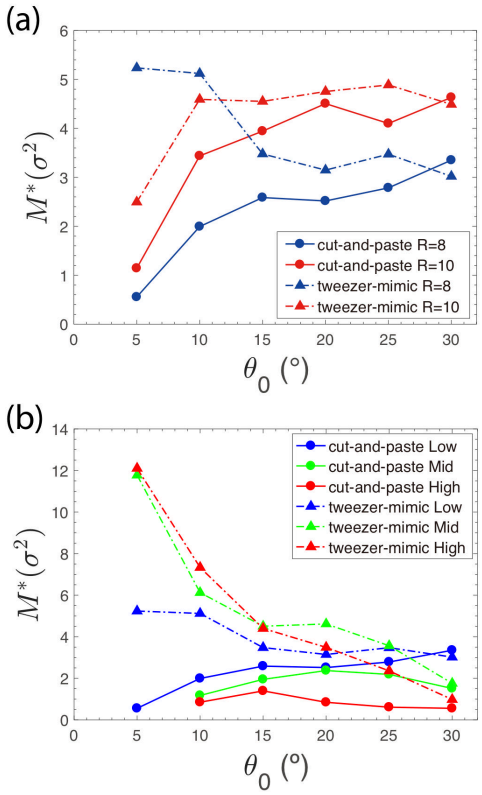

FIG. 4. Mobility at different misorientations (a) in systems with a fixed bulk area fraction at 0.7825; (b) in systems with different bulk area fraction 0.7825 (Low), 0.7973 (Mid) and 0.8209 (High), but with fixed R_0 at 8σ.

To make sense of the 12 sets of conditions at which we have looked at the misorientation-dependent shrinking of GB loops, we start with the lowest of the three pressure conditions studied here (with a bulk area fraction of 0.7825) which is most similar to the systems reported previously.[23] In that work, at a bulk area fraction of 0.7611 the rate of loop closure followed trends in interfacial stiffness. Figures 3 and 4a show average results from simulations of GB loops of two sizes prepared according to two protocols: the cut-and-paste method featured in our previous work and the protocol (described above in Methods section II.C) designed to mimic the

torque by the experimental laser tweezer. Except at two points, the rate of loop closure in this regime correlates to the stiffness, and does not depend strongly on the method of preparation. Such behavior corresponds to the classical regime in which random fluctuations of the GB, made possible by the exchange of dislocations between GB and bulk,[19] are relatively facile but are biased in the direction of shrinking the GB loop to reduce its perimeter. The strength of this bias, which is proportional to the line tension, determines the net rate of motion of the interface in the direction of shrinking the loop. The driving force for θ_0 = 5° is low enough that shrinking is relatively slow.

Exceptional cases are at θ_0 = 5° or 10° for the smaller loop, where preparing the system by rotating a domain rather than by cut-and-paste results in faster shrinking of the GB loop. The initial structures that result from the two preparations are distinct, as shown in Figure 5 (a and b). Under these conditions, the rate of GB loop closure for the cut-and-paste structures varied strongly from trajectory to trajectory. Even for a trajectory whose rate of closure was relatively fast, like the one portrayed in Fig. 5 (a and c), the mechanism differs from the tweezer-mimetic process. Fig. 6a shows that shrinkage of the cut-and-pasted domain involves plastic rearrangement of the spheres through rearrangements that involve changes to the local neighborhoods of a majority of particles in the domain. In contrast, Fig. 6b shows that the process of domain shrinking for the tweezer-mimic domain preserves local neighbor identities except near the border, consistent with an elastic rotation of the core back to its original orientation.

Elastic relaxation was observed experimentally by Lavergne *et al*.[18] for domains below a critical misorientation $\theta^c \approx \frac{3}{\pi}\frac{\sigma}{R}$. At $\theta_0 > \theta^c$, the loops were found to shrink through migration and combinations of dislocations. The crossover in mechanism was shown to originate in a

structural transition: at the critical misorientation, the GB loop supports a hexagonal arrangement of 6 dislocations with a spacing ($\frac{\pi R}{3} = \frac{\sigma}{\theta^c}$) that matches the preferred spacing of dislocations for a GB of that misorientation.[18] The Burgers vectors of the dislocations are aligned perpendicular to the GB, directed towards the center of the grain. At lower misorientation, dislocations also appear at the GB but are oriented with Burgers vectors parallel to the GB, as produced by a simple gliding offset of a pair rows in a hexagonal array.

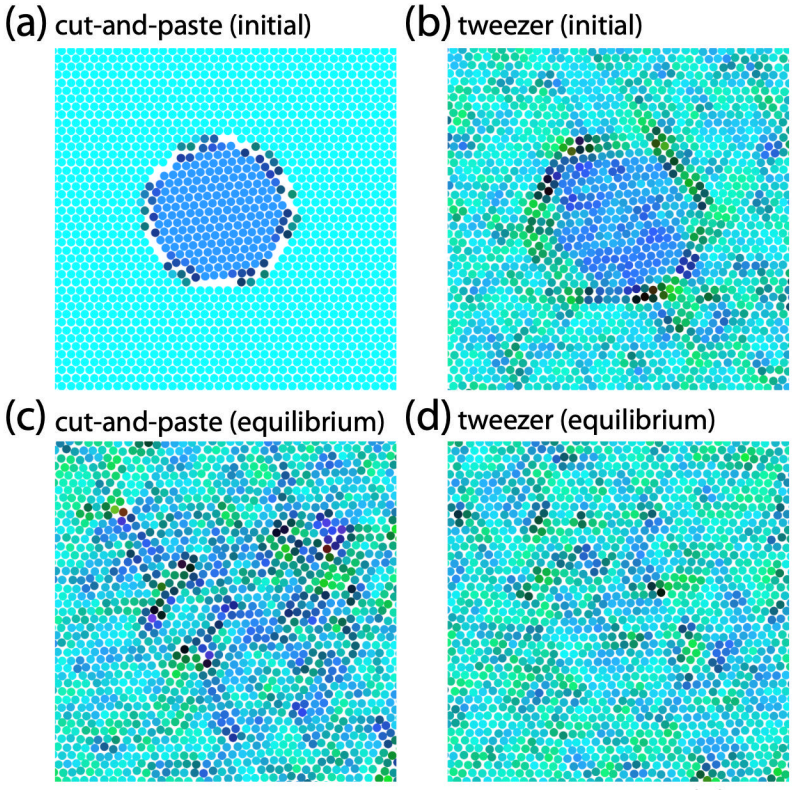

FIG. 5. Snapshots of (a) initial configuration prepared by cut-and-paste method; (b) initial configuration prepared by tweezer-mimic method; (c) configuration after 37000 MC cycles of cut-and-paste structure; (d) configuration after 4000 MC cycles of tweezer-mimic method. Both have initial misorientation $\theta_0 = 5°$, $R_0 = 8\sigma$ and bulk area fraction $\eta = 0.7825$. Degree and phase of orientational order are indicated by color intensity and hue as in ref. [23].

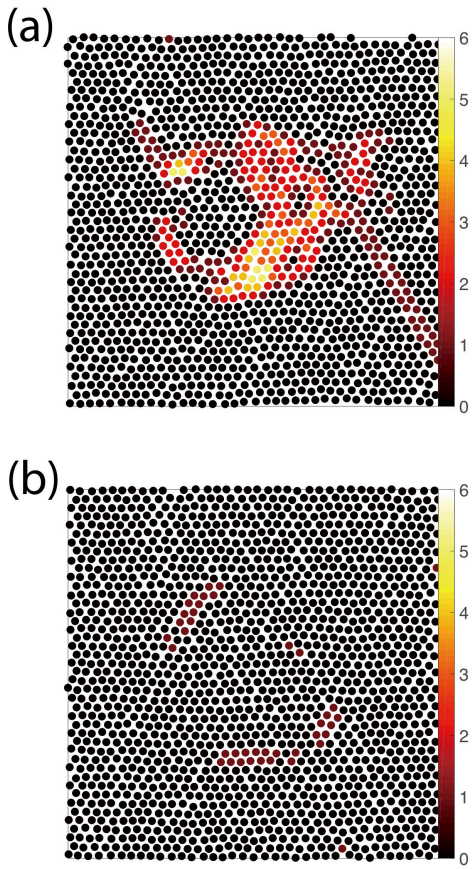

FIG. 6. Number of different neighbors between initial and the last configuration for the system (a) prepared by cut-and-paste method; (b) prepared by tweezer-mimic method. Both have initial misorientation $\theta_0 = 5°$, $R_0 = 8\sigma$ and bulk area fraction $\eta = 0.7825$.

Focusing on the smaller loop size studied, Fig. 4b shows that sensitivity to the preparation of the misoriented domain is greater at higher surface pressure, analogous to lower temperature for a thermal system. At the two higher pressures, simulations reproduce the experimental trend of diminishing mobility at higher misorientation only when the loop is created using the tweezer-mimic method. In contrast, when the domain is created using the cut-and-paste method, the shrinkage at $\theta_0 = 5°$ and higher pressure is too low to measure in the current simulations as the loop persists over the simulation period. The topological difference between typical structures

generated by the two protocols is illustrated through Voronoi diagrams shown in Fig. 7a (generated through the cut-and-paste method) and 7d (generated through the "tweezer-mimic" method and showing displaced rows at the GB).

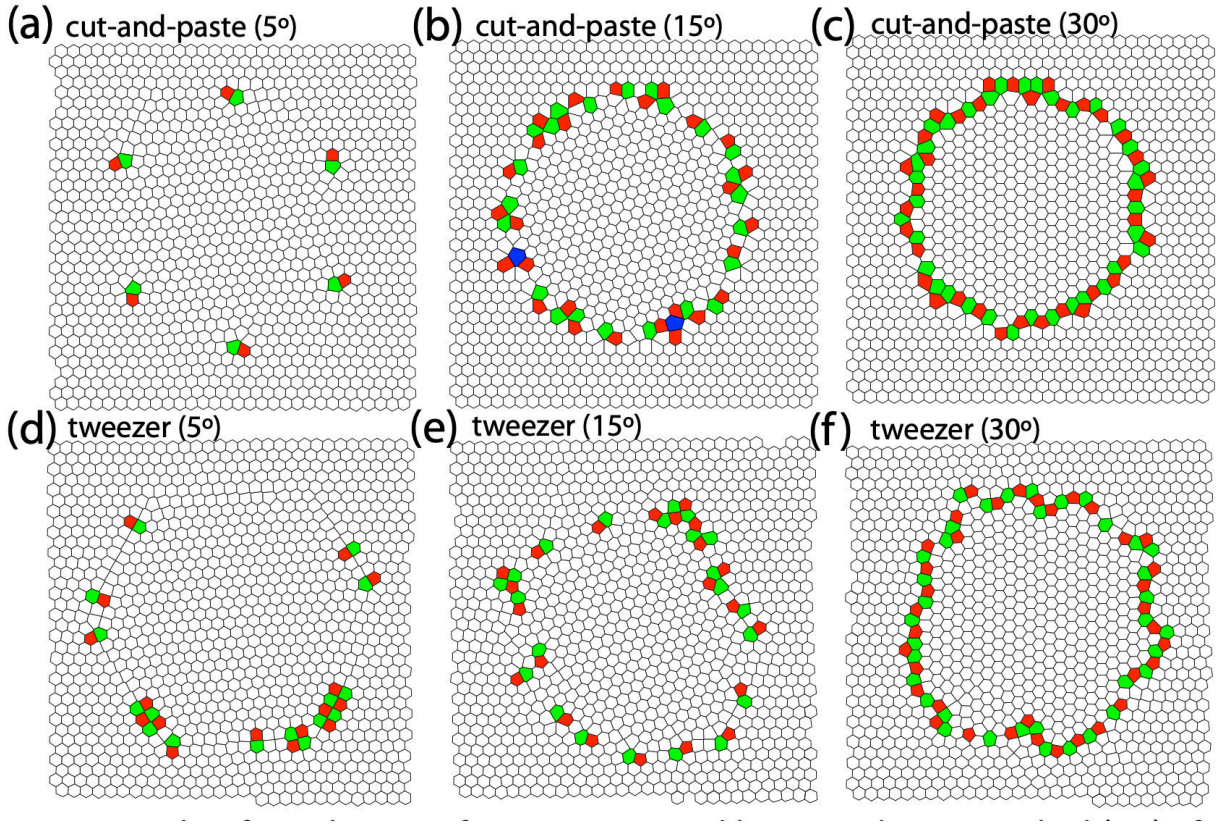

FIG. 7. Voronoi graphs of initial states of systems prepared by cut-and-paste method (a-c) of tweezer-mimic method (d-f) with labelled initial misorientations. All have $R_0 = 10\sigma$ and bulk area fraction $\eta = 0.8209$. Cells are color-coded as pentagon (red), hexagon (white), heptagon (green) and octagon (blue). Adjoined pentagon/heptagon pairs represent dislocations, with Burgers vector along the shared edge.

Both structures were created with the same original dimension of GB loop (R_0=10.0) and $\theta_0 = 5°$, slightly below the nominal critical misorientation $\theta^c = 5.47°$. The structure in Fig. 7(a) stands in apparent contradiction to the structural explanation for elastic-to-plastic crossover presented above. The loop should be too small to accommodate the six dislocations with spacings appropriate to the GB misorientation. What is the "loophole" that permits this loop to exist?

One contribution is that misoriented region grows during the initial relaxation as the surrounding particles fill in the gaps left by the cut-and-paste algorithm. Further inspection shows that it is qualitatively different from the structure presented by Lavergne *et al.*, (Ref. [18], Fig. 3B) in that the dislocations found in our simulations have Burgers vectors that are not directed into the center of the loop but are rotated by 30°. The result is a grain that resembles a 6-sided star (Figure 8) more than a compact hexagon. The GB connecting the defects is not the simple straight boundary on which the preferred spacing of $\frac{\sigma}{\theta}$ is based, and so the structure supports an arrangement of six dislocations even when they are closer to each other than would be stable for a regular hexagon. The dislocation arrangement in turn is the likely explanation for the slow shrinking rate, analogous to the long-lived metastable grain in the 2-d square lattice whose dynamic behavior has been treated theoretically.[6]

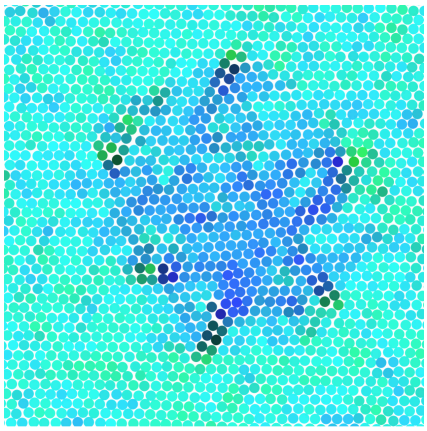

FIG. 8. Snapshot of the GB loop with $\theta_0 = 5°$, $R_0 = 10\sigma$ at high pressure (bulk area fraction 0.8209). Degree and phase of orientational order are indicated by color intensity and hue as in ref. [23]

To remove any doubt that differences in dislocation structure (as opposed to details of our system preparation protocols and Monte Carlo "dynamics") are the origins of the distinct trends, we applied our simulation protocol to a GB loop structure obtained from ref. [18] (see Methods

section II.D.). The 6-dislocation loop, embedded in a defect-free lattice, shrank rapidly during simulation through the migration of dislocations towards its center (Fig. 9, left and center panels, and Movie S1). Once the dislocations came in contact, they recombined into a new pattern with Burgers vectors directed along the perimeter, allowing for concerted rotation of the central core of the loop. This mechanism is evident in the pattern of the neighbor difference map shown in Fig. 9 (right panel), which highlights the gliding paths of the six dislocations and the ring bordering the cluster of fifteen particles in the center that rotated together.

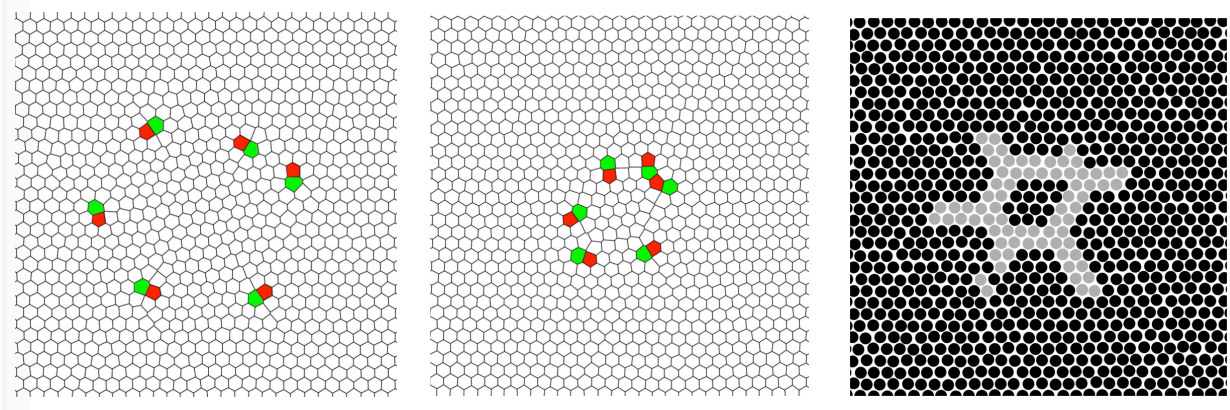

FIG. 9 Left and center: Voronoi representations (as in Fig. 6) of initial experimental θ_0=5° structure from ref. [18], initially and following 176 MC cycles. Right: Structure after closure (250 MC cycles) with particles that have not changed their neighbor list are shown in black, and particles that have 1 new neighbor shown in grey. Trajectory can be viewed in Movie S1.

In contrast, the star-like structure generated by the cut-and-paste protocol shows little change under the same treatment (Fig. 10, left and center, and Movie S2). The dislocations show glide mobility along the direction of their Burgers vectors, but in contrast to those in the experimentally-derived structure (which are attracted to their oppositely-oriented counterparts that lie directly facing them) they appear to experience a weak repulsion. Over a longer simulation trajectory (Fig. 10, right, and Movie S3), the separation between dislocations actually

increases and the star-like aspect of the GB loop becomes less pronounced. Finally, after a total simulation time approximately 100 times longer than the shrinkage time of the experimentally-derived loop, two dislocations approach each other, recombine, and rapidly annihilate two remaining dislocations – leaving a uniformly oriented lattice containing two remaining dislocations (Figure S4 and Movie S4).

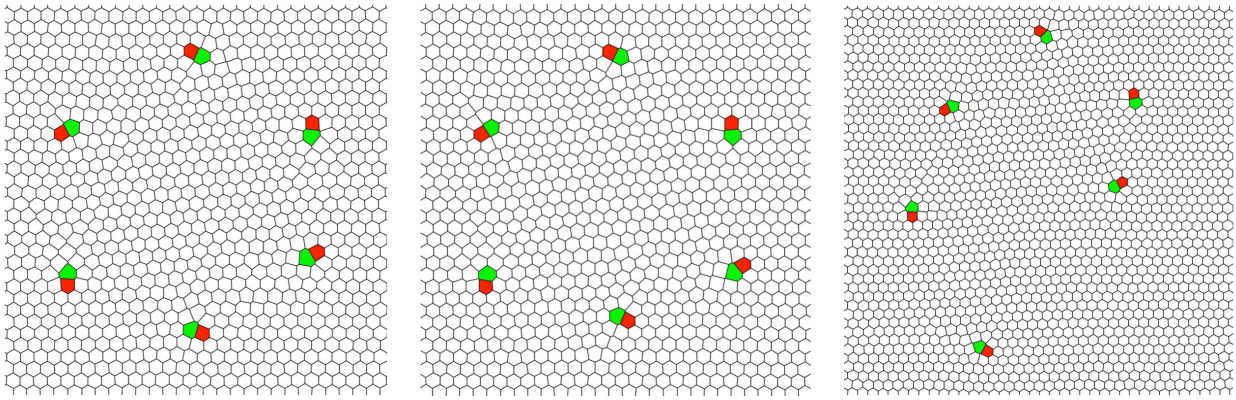

FIG 10. Voronoi representation as in Fig. 6 showing cut-and-paste θ_0=5° structure after initial relaxation (left), after 176 MC cycles (center), and after 16,000 MC cycles (right). Trajectory over first 176 MC cycles can be viewed in Movie S2, over first 16,000 cycles in movie S3, and over final loop closure (16,000-20,000 cycles) in movie S4.

Even when the tweezer-mimic model of preparation is used in simulations, trends in mobility are only partially consistent with the experimental observations of Lavergne *et al*., who found a general relationship over varying initial size R_0 and misorientation θ_0:

$$\frac{1}{M^*} = K(R_0\theta_0 - [R\theta]^c) \qquad (3)$$

In simulations, an approximately linear trend of inverse mobility with θ_0 is followed only for the smaller loops at higher pressures (Fig. 11, panels b and c, dashed blue curves). The larger loops show little dependence of mobility on misorientation, except for a significant slow-down (at medium and high area fractions) at θ_0 = 30°. Even granting that the value of R_0 is somewhat ill-

defined (given relaxation effects discussed in section IIE), this behavior is not consistent with the scaling implied by eq. 3. Adland *et al*. originally proposed the scaling of the inverse mobility with $R\theta_0$ as a consequence of two factors: the rotation of the grain to higher misorientation during shrinking (maintaining fixed $R\theta$ - a process distinct from the elastic *decrease* in θ at fixed R) and a dissipative contribution from this rotation that scales with grain area.[8] The rationalization of this behavior, which was seen in phase-field-crystal simulations for θ_0 up to 15° in a square lattice, is that it preserves the continuity of lattice rows until the final stage of shrinking.[7, 14] (At higher misorientation, an alternative pathway involving dislocation reactions rather than grain rotation was observed.[8,14]) In the lower θ_0 regime, reducing the friction associated with collective rotation of the grain eliminated the strong dependence of mobility on misorientation. There is indirect evidence that collective rotation is associated with lower friction (relative to inter-particle rearrangement) in the simulated systems than in experiment: namely, that the central Gaussian torque component (shown in Figure 1) was not needed to rotate the grain interior, in contrast to the experimental behavior. The origin of this friction in the experiments could be the result of slowly-relaxing interactions between the particles and the substrate. It is therefore tempting to attribute incompatibility of Eq. 3 with the simulation data to this lower friction. It should be noted, however, that rotation of the GB loop to higher misorientation during shrinkage is neither evident in the current simulations (see Fig. 8) nor in the results presented from experiments (see, from Ref. [18], Fig. 1D and Movie S1), so in any case a different justification may be needed to explain the data collapse according to Eq. 3 in experiment.

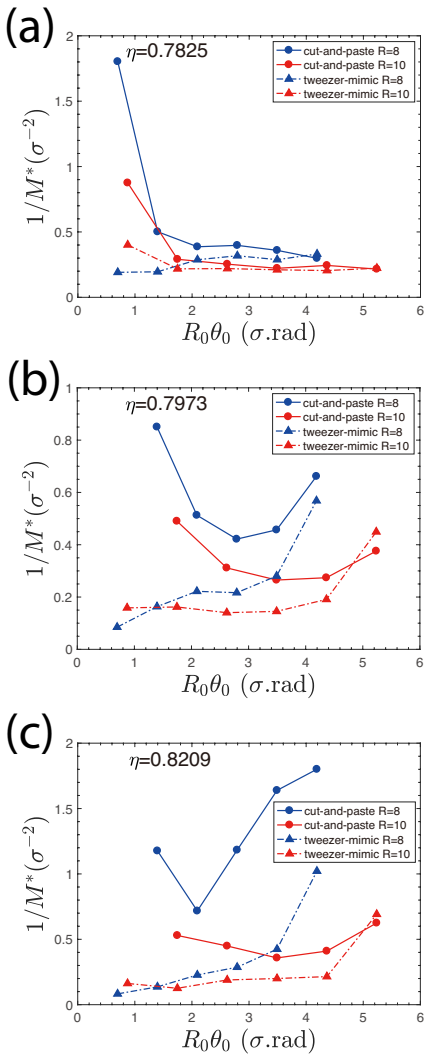

FIG 11. Relation between $1/M^*$ and $R_0\theta_0$ for system (a) at bulk area fraction 0.7825; (b) at bulk area fraction 0.7973; (c) at bulk area fraction 0.8209.

IV. Conclusions

Using a hard-sphere simulation model and a simple Monte Carlo dynamical algorithm, we have reproduced elements of the qualitative behavior of grain boundary loops observed experimentally in 2-d colloidal microspheres. At high enough packing density, GB loops created by rotating a circular region of the 2-d solid to an initial misorientation angle θ_0 showed a crossover from elastic to plastic deformation and a decreasing rate of shrinkage with increasing

θ_0. A qualitatively distinct trend is observed, however, when pressure is lowered enough that the GB can easily fluctuate, or when the GB loop is prepared through a protocol that does not involve a continuous deformation of the structure. A "cut-and-paste" algorithm applied at θ_0=5° produced a simple pattern of six dislocations that is distinct in its dynamical behavior from the pattern created experimentally by laser-tweezer rotation, with orders of magnitude longer lifetime. The cut-and-paste structure might be engineered experimentally by a combining the laser-tweezers rotation with the "optical blasting" method developed by Gerbode *et al*.[21] to melt or remove particles around the border. It remains an open question whether either of these patterns is likely to arise from a more "natural" process, for instance from a grain nucleated inside a disordered region that is embedded in an orientationally mismatched matrix; this would be an interesting topic for future simulations.

Supplementary material

See supplementary material for Figures S1 and S2 containing additional plots of loop closure dynamics, Figure S3 showing system size comparison, Figure S4 showing still frames of loop closure following Figure 10, and movies S1-S4 that accompany figures 9 and 10.

Acknowledgments:

Z. Guo thanks Cong Cao and Jia Song for helpful discussions. Support from the University Research Committee (grant number 00067503) at Emory University is gratefully acknowledged. This work used the Extreme Science and Engineering Discovery Environment (XSEDE) Comet cluster at the San Diego Supercomputer Center, which is supported by National Science

Foundation grant number ACI-1548562, allocation TG-MCB110144. This work also used the resources of the Cherry L. Emerson Center for Scientific Computation.

References:

1. W. W. Mullins, Journal of Applied Physics **27** (8), 900-904 (1956).

2. M. Hillert, Acta Metallurgica **13** (3), 227-238 (1965).

3. G. Gottstein and L. S. Shvindlerman, *Grain boundary migration in metals: thermodynamics, kinetics, applications*. (CRC press, 2009).

4. K. Barmak, E. Eggeling, D. Kinderlehrer, R. Sharp, S. Ta'asan, A. D. Rollett and K. R. Coffey, Progress in Materials Science **58** (7), 987-1055 (2013).

5. P. R. Rios and D. Zöllner, Mater. Sci. Technol. **34** (6), 629-638 (2018).

6. R. Bruinsma, B. I. Halperin and A. Zippelius, Phys. Rev. B **25** (2), 579-604 (1982).

7. J. W. Cahn and J. E. Taylor, Acta Materialia **52** (16), 4887-4898 (2004).

8. A. Adland, Y. Xu and A. Karma, Phys. Rev. Lett. **110** (26), 265504 (2013).

9. D. A. Vega, C. K. Harrison, D. E. Angelescu, M. L. Trawick, D. A. Huse, P. M. Chaikin and R. A. Register, Phys. Rev. E **71** (6), 061803 (2005).

10. E. A. Holm and S. M. Foiles, Science **328**, 1138-1141 (2010).

11. M. Upmanyu, D. J. Srolovitz, A. Lobkovsky, J. A. Warren and W. Carter, Acta Materialia **54** (7), 1707-1719 (2006).

12. Z. Trautt and Y. Mishin, Acta Materialia **60** (5), 2407-2424 (2012).

13. L. Zhang, J. Han, Y. Xiang and D. J. Srolovitz, Phys. Rev. Lett. **119** (24), 246101 (2017).

14. K.-A. Wu and P. W. Voorhees, Acta Materialia **60**, 407-419 (2012).

15. P. Dillmann, G. Maret and P. Keim, Journal of Physics: Condensed Matter **20** (40), 404216 (2008).

16. F. A. Lavergne, S. Diana, D. G. A. L. Aarts and R. P. A. Dullens, Langmuir **32** (48), 12716-12724 (2016).

17. F. A. Lavergne, D. G. A. L. Aarts and R. P. A. Dullens, Phys. Rev. X **7** (4), 041064 (2017).

18. F. A. Lavergne, A. Curran, D. G. A. L. Aarts and R. P. A. Dullens, Proc. Natl. Acad. Sci. **115**, 6922-6927 (2018).

19. S. Deutschländer, C. Boitard, G. Maret and P. Keim, Phys. Rev. E **92** (6), 060302 (2015).

20. M. Liao, X. Xiao, S. T. Chui and Y. Han, Physical Review X **8** (2), 021045 (2018).

21. C. E. Cash, J. Wang, M. M. Martirossyan, B. K. Ludlow, A. E. Baptista, N. M. Brown, E. J. Weissler, J. Abacousnac and S. J. Gerbode, Phys. Rev. Lett. **120** (1), 018002 (2018).

22. G. von Freymann, V. Kitaev, B. V. Lotsch and G. A. Ozin, Chem. Soc. Rev. **42** (7), 2528-2554 (2013).

23. Z. Guo and J. T. Kindt, J. Chem. Phys. **149** (4), 044503 (2018).

24. E. Sanz and D. Marenduzzo, J. Chem. Phys. **132** (19), 194102 (2010).

25. D. R. Nelson, *Defects and geometry in condensed matter physics*. (Cambridge University Press, 2002).

Figure legends:

FIG. 1. Probability distribution of bias moves mimicking LG beam and Gaussian beam in simulations with $R_0 = 8\sigma$.

FIG 2. Shrinking curves showing number *N* of particles inside GB loop created by cut-and-paste method (a) or tweezer-mimic method (b) for initial misorientation 10°, R_0 = 8 σ, at lowest area fraction (0.7825). Different colors represent 16 trajectories initiated with different random number seeds.

FIG 3. Shrinking curves showing number *N* of particles inside GB loop, averaged over 16 trajectories, created by cut-and-paste method (a) or tweezer-mimic method (b) at R_0 = 8 σ and lowest area fraction (0.7825). Initial misorientation angles are indicated by colors given in the legend.

FIG. 4. Mobility at different misorientations (a) in systems with a fixed bulk area fraction at 0.7825; (b) in systems with different bulk area fraction 0.7825 (Low), 0.7973 (Mid) and 0.8209 (High), but with fixed R_0 at 8σ.

FIG. 5. Snapshots of (a) initial configuration prepared by cut-and-paste method; (b) initial configuration prepared by tweezer-mimic method; (c) configuration after 37000 MC cycles of cut-and-paste structure; (d) configuration after 4000 MC cycles of tweezer-mimic method. Both

have initial misorientation $\theta_0 = 5°$, $R_0 = 8\sigma$ and bulk area fraction $\eta = 0.7825$. Degree and phase of orientational order are indicated by color intensity and hue as in ref. [23].

FIG. 6. Number of different neighbors between initial and the last configuration for the system (a) prepared by cut-and-paste method; (b) prepared by tweezer-mimic method. Both have initial misorientation $\theta_0 = 5°$, $R_0 = 8\sigma$ and bulk area fraction $\eta = 0.7825$.

FIG. 7. Voronoi graphs of initial states of systems prepared by cut-and-paste method (a-c) of tweezer-mimic method (d-f) with labelled initial misorientations. All have $R_0 = 10\sigma$ and bulk area fraction $\eta = 0.8209$. Cells are color-coded as pentagon (red), hexagon (white), heptagon (green) and octagon (blue). Adjoined pentagon/heptagon pairs represent dislocations, with Burgers vector along the shared edge.

FIG. 8. Snapshot of the GB loop with $\theta_0 = 5°$, $R_0 = 10\sigma$ at high pressure (bulk area fraction 0.8209). Degree and phase of orientational order are indicated by color intensity and hue as in ref. [23]

FIG. 9 Left and center: Voronoi representations (as in Fig. 6) of initial experimental θ_0=5° structure from ref. [18], initially and following 176 MC cycles. Right: Structure after closure (250 MC cycles) with particles that have not changed their neighbor list are shown in black, and particles that have 1 new neighbor shown in grey. Trajectory can be viewed in Movie S1.

FIG 10. Voronoi representation as in Fig. 6 showing cut-and-paste θ_0=5° structure after initial relaxation (left), after 176 MC cycles (center), and after 16,000 MC cycles (right). Trajectory over first 176 MC cycles can be viewed in Movie S2, over first 16,000 cycles in movie S3, and over final loop closure (16,000-20,000 cycles) in movie S4.

FIG 11. Relation between $1/M^*$ and $R_0\theta_0$ for system (a) at bulk area fraction 0.7825; (b) at bulk area fraction 0.7973; (c) at bulk area fraction 0.8209.